Pergamon

Int. J. Heat Mass Transfer. Vol. 40, No. 5, pp. 1095–1107, 1997

0017–9310/97 $17.00 + 0.00

PII: S0017-9310(96)00135-4

Heat transfer behaviors of a confined slot jet impingement

Z. H. LIN, Y. J. CHOU and Y. H. HUNG†

Department of Power Mechanical Engineering, National Tsing Hua University, Hsinchu, Taiwan 30043, Republic of China

(*Received* 6 *September* 1995 *and in final form* 19 *April* 1996)

Abstract—An experimental study on heat transfer behaviors of a confined slot jet impingement has been systematically performed. The parametric effects of jet Reynolds numbers and jet separation distance on heat transfer characteristics of the heated target surface are explored. With the measurement of jet mean velocity and turbulence intensity distributions at nozzle exit, two jet flow characteristics at nozzle exit, initially laminar and transitional/turbulent regimes, are classified. As for the investigation of heat transfer behaviors on stagnation, local and average Nusselt number, it is evident that the effect of jet separation distance is not significant; while the heat transfer performance increases with increasing jet Reynolds number. Comparisons of the present experimental data with the existing numerical and experimental results are made. Besides, two new empirical correlations for stagnation and average Nusselt numbers on the heated target surface are also reported in the study. Furthermore, a concept of effective cooling length is introduced to evaluate the average Nusselt number on a finite-length target surface, the existing numerical results are reasonably consistent with the present experimental data. Copyright © 1996 Elsevier Science Ltd.

INTRODUCTION

The demand for compactness and higher operational speeds leads to high power density in electronic packages. The thermal management of compact electronics packages, a formidable task, is essential for reliability and efficiency of operation. Improvements in cooling methods are required to avoid unacceptable temperature rise. A heat transfer enhancement technique of jet impingement with low air velocity, to meet the limitation of the resulting force of air jet exerted on the package, is a promising way to achieve higher thermal performance for compact electronics packages. A low turbulence jet with low velocity is sometimes referred to as 'laminar' jet since nozzle designs are employed to reduce turbulence [1].

Commonly, two kinds of jet configuration are employed in the existing study, that is, circular and slot jets. From the survey of existing literature, it may be found that one drawback in using a single circular jet is the concentration of cooling in the small impingement zone of the heated surface. The use of multiple jets enhances cooling uniformity by creating several impingement zones which cover a significant fracture of the heated surface. Nevertheless, multiple jets promote flow blockage between the jets and complicate fluid distribution downstream from the impingement zone. These problems become critical in the cooling of multi-chip modules, which require uniform cooling of a large number of chips as well as ease of fluid introduction into, and rejection from, the module in the smallest volume possible. To overcome the above problems, Wadsworth and Mudawar [2] performed an experimental cooling study for a stimulated multi-chip module by means of a confined two-dimensional slot jet. They found that a potential solution to these problems was to use a two-dimensional or slot jet which provided a larger impingement zone and ensured uniform coolant rejection following impingement. In addition, cooling via a two-dimensional slot jet maintains nearly isothermal chip surface conditions. Therefore, a two-dimensional or planar air jet obviously offers some beneficial features, such as, cooling effectiveness, uniformity and controllability on compact electronic packages.

As we know, in recent years, most of the leading manufacturers of computers and other microelectronics equipment have begun to develop the technology and packaging strategies needed to insert multi-chip modules into their product families. Several companies have chosen to emphasize relatively small modules containing 4–10 small chips on a common substrate, while many other companies have pursued the development of substantially larger modules containing from 30 to as many as 133 chips.

Table 1 lists the thermal features of some famous air-cooled multi-chip modules [3]. Based on this information, the multi-chip modules cooled with a slot jet impingement may be classified into two package types as shown in Fig. 1(a). From the results of Wadsworth and Mudawar, mentioned in the last paragraph, the module with high-density chips can be simulated as

† Author to whom correspondence should be addressed.

NOMENCLATURE

A	area of heated target surface
D	hydraulic diameter of jet nozzle, $2W\ell/(W+\ell)$
H	separation distance
H_e	effect cooling function
h_s	stagnation heat transfer coefficient
h_x	local heat transfer coefficient
k	thermal conductivity of air
L	nozzle length
L_e	effective cooling length
L_H	length of heated surface
ℓ	nozzle depth
Nu_s	Nusselt number at stagnation line, $h_s L_H/k$
Nu_x	local Nusselt number, $h_x L_H/k$
Pr	Prandtl number, ν/α
Q_m	flow rate of air
Q	heat dissipation rate
q''	heat flux, Q/A
Re_D	jet Reynolds number, $\bar{\bar{V}}_j D/\nu$
T_j	jet exit temperature
$T_{w,x}$	local wall temperature
Tu	turbulence intensity
V	streamwise velocity; voltage
$\bar{V}$	mean streamwise velocity
$\bar{\bar{V}}_j$	volume-weighted mean streamwise velocity at nozzle exit
v'	fluctuating velocity component
W	nozzle width
X, Y	coordinates shown in Fig. 1(b)
Z	normal distance measured from nozzle exit, $H-Y$.

Greek symbols

α	thermal diffusivity of fluid
μ	dynamic viscosity of air
ν	kinematic viscosity of air.

Superscripts

$\bar{}$	mean
$\bar{\bar{}}$	volume-weighted mean.

Subscripts

c	center-line; convection
e	effective
k	conduction
i	internal-energy change
r	radiation
s	stagnation line
t	total heat input.

an isoflux or nearly isothermal heating plate. The geometric configuration for air cooling of a stimulated module with a confined impingement slot jet may then be simplified as shown in Fig. 1(b).

According to the literature survey [4], most results reported in existing literature emphasized the fluid flow and heat transfer characteristics of impinging jets without confinement. Information on fluid flow and heat transfer characteristics for slot jet impingement in a confined space, is scarce. No data related to jet flow characteristics at jet nozzle exit, such as jet mean velocity profile and turbulent intensity which play an important role in influencing heat transfer behaviors, were mentioned in the existing literature. Furthermore, other important factors, such as jet Reynolds number and jet separation distance, affecting the heat transfer behaviors of confined slot jet impingement have not been systematically investigated.

More recently, Chou and Hung [5, 6] presented a series of numerical results for impingement cooling of an isothermally heated surface with a confined laminar slot jet. The effects of jet Reynolds number, ratio of jet separation distance to jet width and jet exit velocity profile on heat transfer characteristic of the heated target surface, were explored. New correlations for stagnation and local Nusselt numbers along the heated surface were reported in their study. These correlations gave satisfactory agreements with other existing theoretical results. Nevertheless, in the existing studies, the numerical results in such a jet configuration generally underpredicted the corresponding experimental data. For instance, the difference between the predicted and the measured results ranged from 16 to 44% in the study of Schafer *et al.* [7]. This discrepancy between calculated and measured results may be attributed to variable fluid properties, the three-dimensional effects, the possible influence of buoyancy and/or turbulence in the experimental system. In order to advance our fundamental understanding on the topic, a series of systematic exper-

Table 1. Thermal features for famous air-cooled multi-chip modules

Module type	Chip size (mm)	Chip power (W)	Module size (mm)	Module power (W)
IBM 4381 module	4.6 × 4.6	3.8	64 × 64 × 40	90
Mitsubushi HTCM	8.0 × 8.0	4.0	66 × 66 × 22	36
Hitachi SC RAM module	1.9 × 4.0	1.0	27.4 × 27.4 × 16	6
AT&T WE32100 MICROPAC	10 × 10	1.0	13 × 13 × 15	3

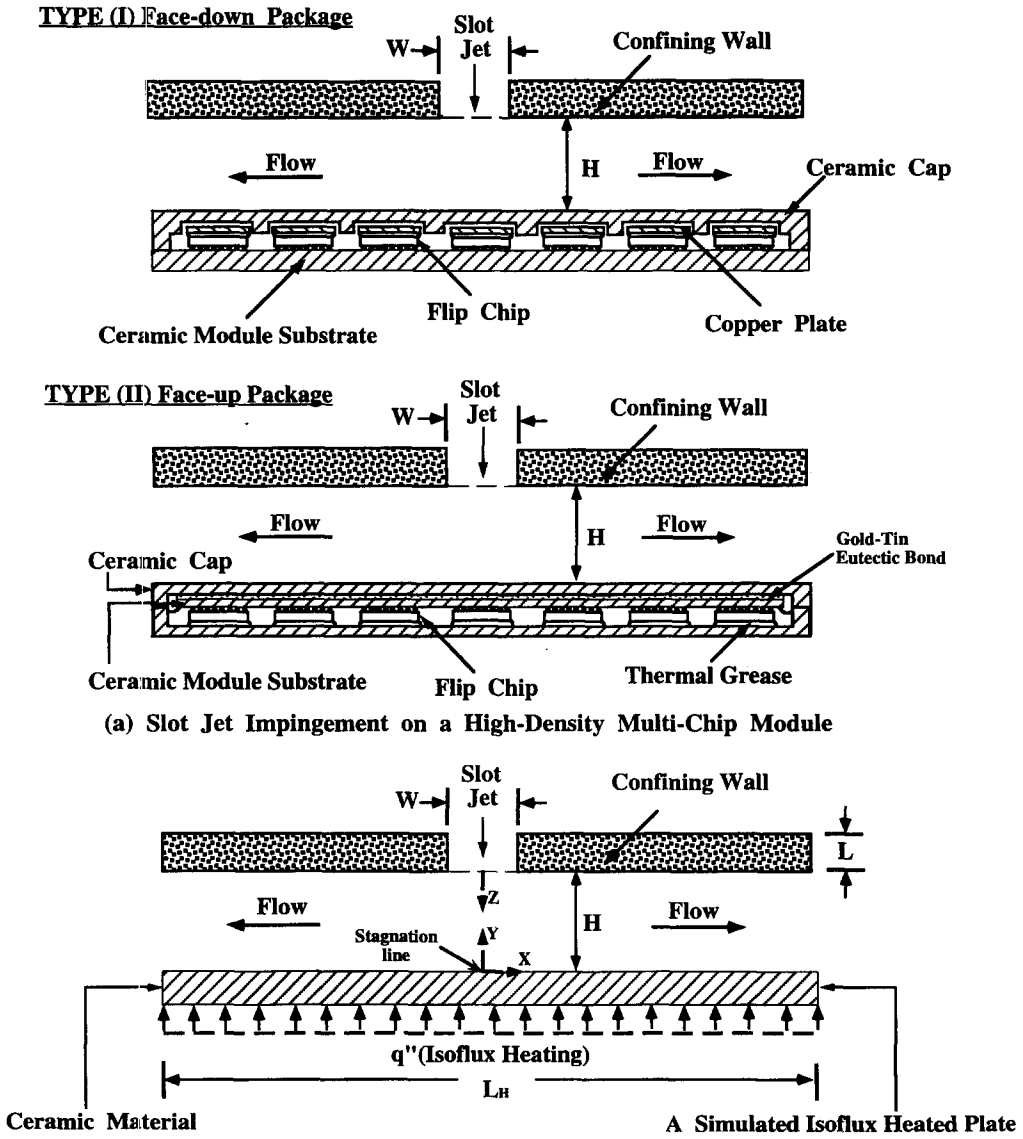

Fig. 1. Slot jet impingement on a high-density multi-chip module.

iments have been conducted. The objectives of the present study include: (1) to classify the jet flow characteristics at nozzle exit; (2) to explore the effects of jet Reynolds number and jet separation distance on stagnation, local and average heat transfer characteristics in confined slot-jet impingement problems; (3) to propose new empirical correlations for evaluating stagnation and average heat transfer characteristics and (4) to compare the present experimental data with existing theoretical and experimental results.

THE EXPERIMENTS

Figure 2 shows the overall experimental setup with relevant apparatus and instruments. The measurements for the present experiments are performed in a symmetric mode and the acquisition of all the experimental data is in steady state. The present experimental facilities are composed of three major parts, i.e. (1) air supply system; (2) heated target plate and (3) apparatus and instrumentation. Brief descriptions of general configuration and functions of the facilities are introduced in the following.

Air supply system

The air for impinging on the heated target surface is supplied by a reciprocating compressor system. Air is compressed and stored in a 304 l air tank at a specified pressure for eliminating air surge. When the experiment is operated, the compressed air flows through an air dryer and an oil strainer for water and oil separations, respectively. Air flow rate is controlled and measured by two precise Hasting mass flow con-

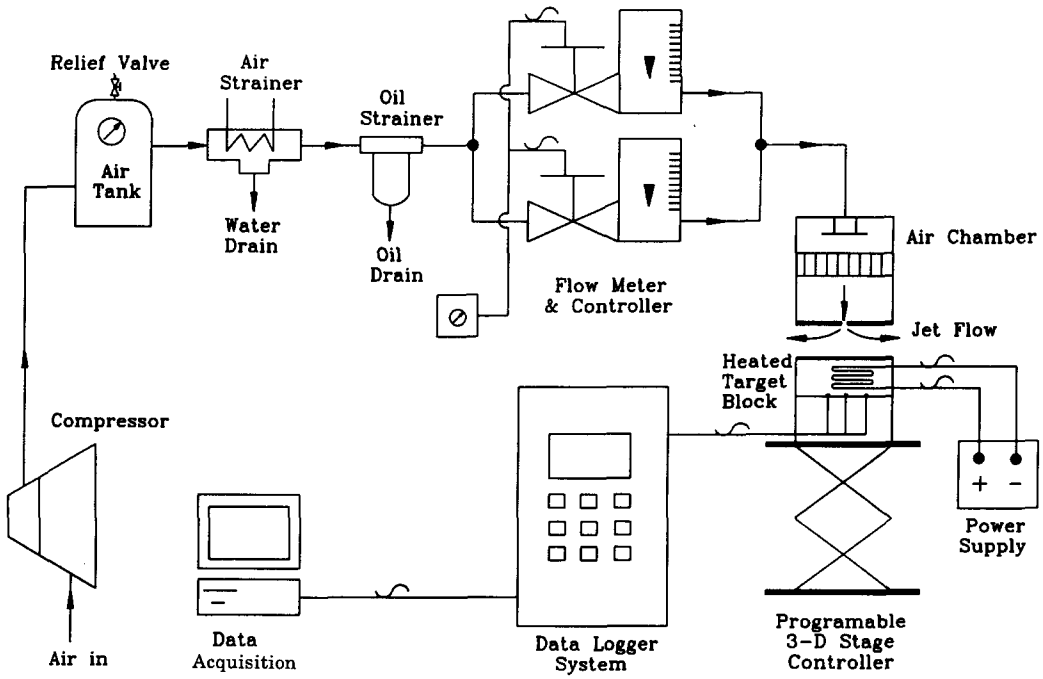

Fig. 2. Overall experimental setup with relevant measurement systems.

trollers (Models: HFC-202F and HFC-203C). To obtain accurate flow rate, the measured flow rate should be compensated due to the temperature effect with a factor of 0.2%/°C, which was suggested by the manufacturer of the mass flow controller. The accuracy and the repeatability of these two controllers are $\pm 1\%$ (F.S.) and $\pm 0.2\%$ (F.S.), respectively. Finally, a flexible tube at the end of the air supply system is connected to an air jet chamber, which will be introduced in the next section.

Air jet test chamber

As shown in Fig. 3(a), the assembly of the air jet test chamber in the experiment is composed of two air plenums. The upper plenum is made of 2 cm thick acrylic–plastic material which is 30 cm long and the internal cross section is 10×10 cm. It is designed to provide a controllable and stable jet impinging the heated target surface. There is a momentum dissipation plate with a size of $5 \times 5 \times 0.5$ cm in dimension to dissipate the axial momentum of the air flow from the air supply system. A 5 cm thick honeycomb is designed to create a uniform air flow with low turbulence. The lower plenum is designed and constructed for the flexibility in interchanging different slot nozzle configurations. The contact area between these two plenums is sealed with an O-ring for preventing the leakage of the pressurized air into the air jet test chamber. In the present study, the slot width of the square-edged nozzle is fixed at 5.0 mm, and the ratio of the nozzle length to nozzle width is designed to be 1. Besides, in order to ensure a two-dimensional flow configuration, the air flow is restricted with two 1.8 cm thick acrylic–plastic shields between air chamber and the heated target surface in the spanwise direction.

Heated target block

The air jet generated from the air jet chamber normally impinges onto the center of a heated target block. To simulate a practical MCM module size listed in Table 1, the schematic of the heated target block composed of four layers is shown in Fig. 3(b). The size of the heated target block is 10 cm wide, 11 cm long, and 4 cm thick. The first layer is the heated target surface, made of 1 mm thick stainless steel sheet (AISI 304) with a size of 6.7×6.7 cm. It is polished to minimize the surface roughness and emissivity, hence lessen radiative heat losses. The selection of using stainless steel sheet (AISI 304) in the study is mainly based on that the thermal conductivity of AISI 304 ($k = 14.6$ W m^{-1} K^{-1}) is almost the same order as that of alumina (Al_2O_3, $k = 18$–20 W m^{-1} K^{-1}) [8, 9]. The second layer is a 6.7×6.7 cm thermofoil heater with a thickness of 0.03 cm, expoxied on the inner surface of the first layer. The thermofoil heater, which can be applied to a voltage range of 0–60 V with an electric resistance of 380–382Ω, is used for heating the stainless steel test surface. With a real-time infrared thermography system (AGEMA Model Thermovision 486), the emissivity of the stainless steel test surface was measured and calibrated to be 0.17 in the present experiments. There are 33 calibrated T-type thermocouples installed for measuring the local temperatures of the heated target surface. The third layer is a 2.8 cm thick balsa slab, which is expoxied on the backside of the thermofoil heater to inhibit conductive heat

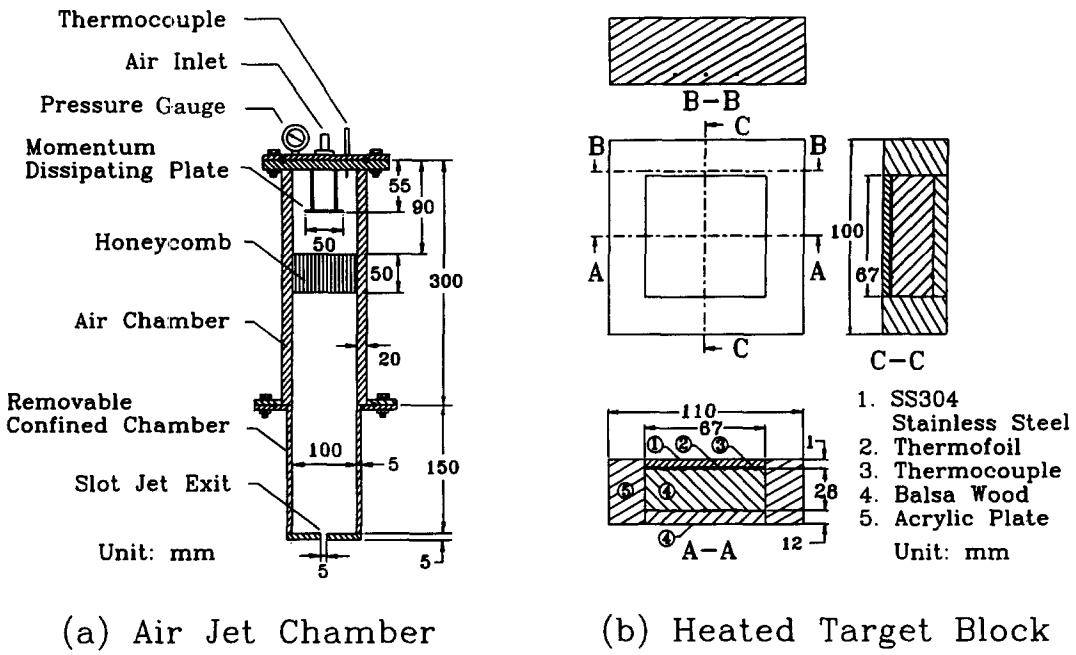

Fig. 3. Schematics of air jet chamber and heated target block.

losses from the heaters. At the backside of the balsa slab, there are nine calibrated T-type thermocouples installed to estimate the conductive heat losses. The outer layer (i.e. the fourth layer), expoxied on the backside of balsa slab is a 1.2 cm thick balsa slab. Fine holes with a diameter of 0.2 cm are drilled through the balsa and the outer layer acrylic–plastic hollow cuboid to allow the passage of heater leads and thermocouples. There are a total of 67 calibrated thermocouples installed for local temperature measurements of the heated target block.

The test target block is placed on a programmable motor-driven three-dimensional (3-D) precision stage controller. The 3-D stage controller is used to precisely adjust the position of the test target surface and the jet separation distance between nozzle exit and test target surface. The minimum movement for position control of the test target surface with this system is estimated to be 10 μm. Moreover, the horizontal of the test target surface is measured with a four-point alignment level (Model: CIC-39381, accuracy $\pm 0.2°$) and adjusted by four screw-driven legs of a flat table, which supports the 3-D stage controller.

Apparatus and instrumentation

In the measurement of mean velocity and turbulence intensity distributions at nozzle exit, a TSI hot-wire anemometer (Model 1500-2SH) with a single-wire sensor (Model 1260A-T1.5) is used. The sensor is supported and grabbed by a programmable motor-driven 3-D stage controller. The 3-D stage controller is used to adjust the measuring position of the hot-wire sensor. The minimum movement for position control with this system is estimated to be 10 μm. The data measured from the single-wire sensor in the experiments are digitized by the TSI FlowPoint system with A/D converter and velocity transducer. With this system, the data can be transferred into mean velocity and turbulence intensity. In the present experiment, a total of 1024 independent samples at a rate of 1000 Hz are taken at each position. Besides, the air temperature at nozzle exit can also be measured with a calibrated T-type thermocouple installed in the velocity transducer system for velocity calibration. The maximum deviation of the present measured velocity data from those obtained with a standard TSI calibrator (Model 1125) is 6.02%.

As for temperature measurement, the local temperature distributions on the test surface can be accurately measured with 67 calibrated T-type thermocouples embedded at the specified locations of the target block. Additionally, the jet exit temperature can be also measured with a calibrated T-type thermocouple. All the local temperatures as well as jet exit temperature can be measured with a FLUKE-2280B data logger system interfaced to PC–AT based peripherals.

Experimental procedures

Prior to the operation of the experiments, all the measuring instruments are calibrated and the air jet chamber and the target block are horizontally and properly installed in the test section. The experimental procedures include the following steps in an experimental sequence: experimental preparations; initial temperature measurement; jet separation distance adjustment; air flow rate selection; mean velocity and turbulence intensity measurement at nozzle exit; input heating power measurement and temperature measurement in the steady-state periods.

Data reduction

The measurements in the present experiments can be divided into two categories, namely, air jet flow rate and surface temperature measurements. The jet Reynolds number is determined by the air flow rate which is controlled and measured by two Hasting mass flow controllers. The accuracy and repeatability of the flowmeter are $\pm 1\%$ (F.S.) and $\pm 0.2\%$ (F.S.), respectively. Consequently, the average jet velocity and Reynolds number can then be easily evaluated with the measured air flow rate. The jet volume–weighted mean streamwise velocity and jet Reynolds number can then be calculated with the following equations, respectively,

$$\bar{\bar{V}}_j = Q_m/(W\ell) \tag{1}$$

and

$$Re_D = \rho \bar{\bar{V}}_j D/\mu \tag{2}$$

where D is the hydrodynamic diameter of the slot nozzle, $2W\ell/(W+\ell)$.

For exploring heat transfer characteristics, a further data reduction is needed to transfer temperatures to heat transfer information. The objective of the data reduction in the experiments is to get the local and average heat transfer coefficients on the target surface, using an effective model to calculate the heat losses of the test block and to obtain an accurate convective heat flux.

For evaluating the convective heat flux dissipated from the heated target surface, based on the energy conservation concept, it may be proposed that the total heat generated by the thermofoil heater Q_t is converted into the following four heat-transfer modes in the experimental period: (1) radiative heat loss, Q_r; (2) conductive heat loss, Q_k; (3) convective heat dissipated from the target surface, Q_c and (4) internal-energy change of the stainless steel sheet and balsa wood, Q_i. That is

$$Q_c = Q_t - Q_r - Q_k - Q_i. \tag{3}$$

This energy-balance equation calculates the net convective heat, Q_c, dissipated from the target surface to the air jet in the confined channel. The total power input to heater is Q_t which equals V^2/R. Here V represents the output voltage of the d.c. power supply and R is the resistance of the thermofoil heater. Q_r is the radiative heat loss from the stainless steel surface to its surroundings. It is evaluated with thermal diffuse gray-body networks. According to the results of the radiation analysis, the maximum radiative heat loss is less than 5.06% of the total input power for all the cases considered in the present study. Q_k is the conductive heat loss to the insulated balsa slab. It is evaluated by a two-dimensional conduction models. The Q_k value varies from 0.68 to 17.26% of the total input power in the present experiments. Q_i is the internal-energy change of the stainless steel sheet and the balsa wood during the experimental period. The method for the evaluation of internal-energy change Q_i had been introduced in Ref. [10].

Before the experimental results of the steady-state condition are displayed, it is necessary to clarify the steady-state of each experiment. Usually, the steady-state condition is considered to be achieved when Q_i approaches zero, the Q_r and Q_k reach their steady-state values, respectively, and the Q_c variation with time is less than 1.0% of the previous Q_c value in each experiment. In general, the steady-state condition can be achieved about 45 min after the power is turned on. After Q_t, Q_r, Q_k and Q_i are evaluated, the net convective heat dissipation rate from the stainless steel surface, i.e. Q_c can then be obtained. Afterwards, the local and average heat transfer coefficients and Nusselt numbers at the specified locations in the steady-state period are finally calculated. Furthermore, in order to ensure the repeatability for experimental data, three sets of data were obtained under the same experimental conditions for each case. The maximum deviation is less than 4.95% in the present study.

Uncertainty analysis

The uncertainty associated with the experimental data is estimated using the standard single-sample uncertainty analysis recommended by Kline and McClintock [11] and Moffat [12]. In the present experiments, the temperature measurements were accurate to within $\pm 0.2^\circ$C, the uncertainty of the convective heat flux q_c'' is estimated to be 2.65% and those of Re_D and Nu for the ranges of parameters studied in the steady-state period are within 1.68 and 5.54%, respectively.

RESULTS AND DISCUSSION

The main emphasis of the present study is on heat transfer characteristics of a confined slot jet. The schematic of the confined jet test section with relevant definition of parameters is shown in Fig. 1(b). A series of experimental investigations are conducted for exploring the flow and heat transfer characteristics in such a jet configuration. Two parameters varied in the study are the ratio of separation distance to nozzle width and jet Reynolds number. The ranges of the above parameters investigated are $H/W = 1$–8 and $Re_D = 190$–1537. In the present study, the length of the confinement region is designed as 11.0 cm and the ratio of nozzle length to width (L/W) is fixed as 1.0. The power of the thermofoil is controlled at 22–35V and the resistance of the thermofoil ranges between 380 and 382Ω. Thus, through the data reduction with equation (3), the convective heat dissipated from the target surface ranges from 275–718 Wm^{-2}. The surface temperature distributions are measured with calibrated thermocouples and they range between 40 and 70°C. The ambient temperatures in the experiments vary between 21 and 26°C. Forty-two data sets for cases with various above-mentioned parameter combinations are obtained. In addition, the jet exit tem-

perature T_j is usually chosen as a reference to correct jet velocity measurement and to explore heat transfer behavior on the heated target surface in the present study.

Definition of heat transfer parameters

According to the definition of Newton's law of cooling, the local convective heat transfer can be expressed as

$$h_x = \frac{q''_c}{T_{w,x} - T_j} \tag{4}$$

where $T_{w,x}$ and T_j represent the local wall temperature and jet exit temperature, respectively. q''_c is the local convective heat flux, Q_c/A.

Thus, the local and stagnation Nusselt numbers can be evaluated, respectively as,

$$Nu_x = \frac{h_x L_H}{k} \tag{5}$$

and

$$Nu_s = \frac{h_s L_H}{k} \quad \text{at} \quad X = 0. \tag{6}$$

The average heat transfer coefficient on the heated target surface in the study can then be evaluated with the following equation.

$$\bar{h} = \frac{1}{L_H}\int_{L_H/2}^{L_H/2} h_x \, dX = \frac{q''_c}{L_H}\int_{L_H/2}^{L_H/2} \frac{1}{T_{w,x} - T_j} dX \tag{7}$$

where the integration of equation (7) is approximated by summing up all products of the reciprocal of local temperature difference and the corresponding length of segment ΔX in the present experiments.

Accordingly, the average Nusselt number based on the length of heated target surface can be defined as

$$\overline{Nu} = \frac{\bar{h} L_H}{k}. \tag{8}$$

Jet flow characteristics at nozzle exit

To classify the jet flow conduction at the nozzle exit, both the jet mean velocity distribution and the corresponding turbulence intensities at nozzle exit are explored. The results are discussed in the following.

Velocity distribution. The effect of jet Reynolds number on the jet mean velocity distributions at 1.0 W from the nozzle exit, i.e. $Z/W = 1$, is shown in Fig. 4. In this figure, the mean streamwise velocity distributions are plotted in a dimensionless form of $\bar{V}/\bar{V}_c$, where $\bar{V}$ is the local mean streamwise velocity at a specific X/W location and $\bar{V}_c$, the centerline mean streamwise velocity. Besides, the profiles of uniform and parabolic lines are also plotted in the figure for comparisons. The results show that the present mean velocity at nozzle exit is developing; additionally, they also reveal that the entrainment effect of the jet itself and ambient fresh air is not significant at a lower Reynolds number, say $Re_D < 1226$; while the jet is

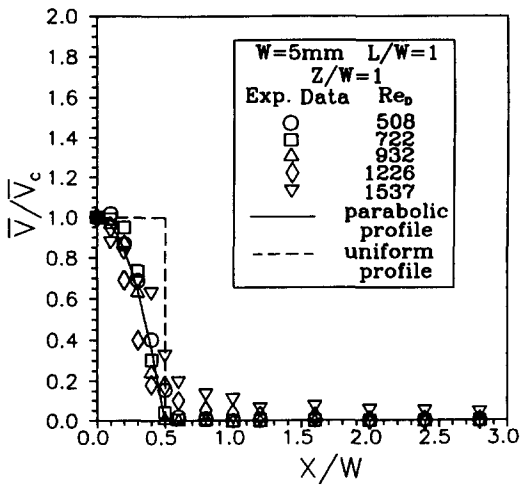

Fig. 4. Effect of jet Reynolds number on distribution of jet streamwise mean velocity flow at $Z/W = 1$.

significantly affected by the ambient air at a higher Reynolds number, say $Re_D \geqslant 1226$.

Turbulence intensity distribution. In the present study, the distributions of turbulence intensity (Tu) at 1.0 W from the nozzle exit (i.e. $Z/W = 1$) for various Reynolds numbers are measured with a TSI hot-wire anemometer. A good index to explore the initial jet flow condition at nozzle exit is the turbulence intensity on the jet centerline at $Z/W = 1$. The reason is that the turbulence intensity at this location near the nozzle exit is not significantly affected by the surrounding ambient air in the present experimental range of $Re_D = 190$–1537.

As we know, if any one quantity is to be used to describe how turbulent the flow is, the turbulent kinetic energy or turbulence intensity is the most logical choice [13]. Generally, the flow characteristic of a jet with its centerline turbulence intensity less than 5% at nozzle exit it can be considered as initially laminar. From the present experimental results, it is obviously found that all the turbulence intensities for the cases of $Re_D < 1226$ are less than 5% at $X/W = 0$. This manifests that the interaction interaction of jet itself and surrounding ambient air is insignificant at a low Reynolds number. Accordingly, the jet at a Reynolds number smaller than 1226 may be regarded as in an 'initially' laminar flow regime. As the Reynolds number gradually increases, say $Re_D \geqslant 1226$, the turbulence intensities at $X/W = 0$ are sharply increased. It should be noticed that the air jet issues from a sharp edged short slot nozzle in the present experiments. Accordingly, this specific nozzle configuration will give a much different jet than a jet issued from a long straight pipe or a nicely shaped nozzle. Due to the sharp edges, recirculation patterns exist that have influence on the turbulence development of the jet, especially for the case with a high jet Reynolds number, say $Re_D \geqslant 1226$. As expected, a higher measured turbulence intensity of 10–18% can be found.

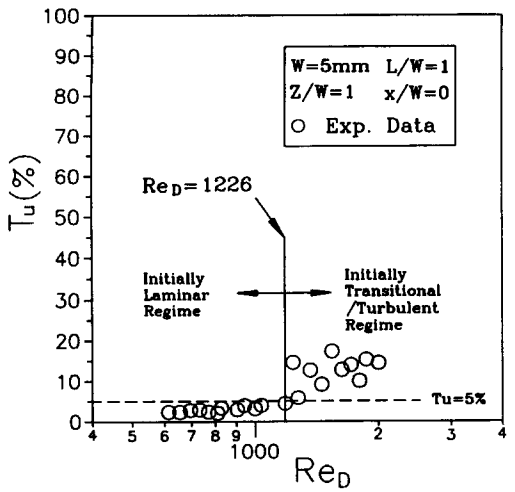

Fig. 5. Initial jet flow characteristics are $Z/W = 1$ for various jet Reynolds numbers.

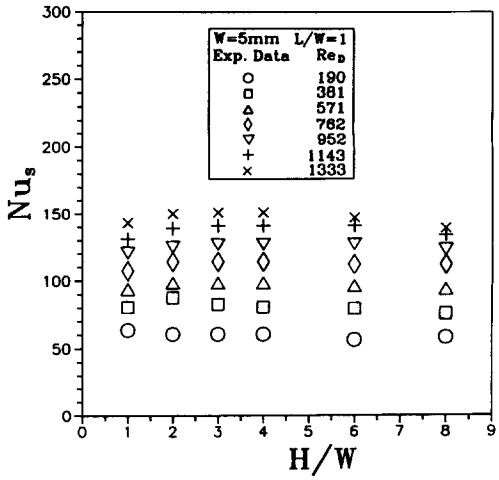

Fig. 6. Effects of Re_D and H/W on stagnation Nusselt number.

This is most probably due to the specific configuration. In addition to the effect of nozzle configuration, the experimental results also reveal that there is a significant interaction, due to the shear generated by the velocity gradient between the jet and the surrounding ambient air, in the region of mixing layer. Consequently, the high turbulence occurring in the region of the mixing layer will diffuse more easily to the region nearby the centerline of the jet. Therefore, the jet flow characteristics at nozzle exit for the cases of $Re_D \geqslant 1226$ may be considered as in an 'initially' transitional/turbulent regime.

In summary, based on the experimental results, two jet flow characteristics at nozzle exit, an initially laminar regime and a transitional/turbulent regime, are classified in Fig. 5. For $Re_D < 1226$, it may be regarded as in an initially laminar jet flow regime because of a very low turbulence intensity at nozzle exit. As $Re_D \geqslant 1226$, it may be considered as in an initially transitional/turbulent regime because of an unsteady behavior with a significantly high turbulence intensity for $Re_D \geqslant 1226$. The present conclusion is consistent with the results reported by McNaughton and Sinclair [14]. They presented the transitional regime for round-jet patterns occurred at $Re_D = 1000$–3000.

Stagnation heat transfer characteristics

Figure 6 shows the effects of the ratio of jet separation distance to nozzle width, H/W, on the stagnation Nusselt number with various jet Reynolds number of $Re_D = 190$–1537. This figure illustrates the effect of H/W on the stagnation heat transfer is not so significant as that found in the numerical study reported by Chou and Hung [6]. The stagnation Nusselt number remains invariant especially in the case of lower jet Reynolds number as it is depicted in this figure. As the jet Reynolds number increases, the stagnation Nusselt number distribution will become a slightly convex shape. A similar phenomenon can be found in Sparrow and Wong's study [15]. However, the present experimental trend is different from the numerical results presented by Chou and Hung. In Chou and Hung's study, the stagnation heat transfer monotonically decreases with increasing H/W ratio. This discrepancy may be caused by the assumption of laminar flow made in the numerical study. According to the characteristics of laminar flow, the flow is smoothly changed unless the jet Reynolds number exceeds a critical value. When the jet Reynolds number exceeds a critical value, a complicated turbulent model is needed to handle this situation. Consequently, the discrepancy of phenomenon between the present experimental data and the theoretical results may be explained by the interactive effect between the increase of turbulence intensity and the diminishment of jet center-line velocity due to the presence of the confinement plate and the H/W variations.

In the present experiments, the interactive effect between the increase of turbulence intensity and the diminishment of jet velocity along the center line of the slot jet is shown in Fig. 7. Immediately on leaving the slot nozzle, the air in the jet begins to entrain the surrounding confined still air. The width of the mixing region increases continuously and at some distance from the nozzle exit it is wide enough to have penetrated to the center line of the jet. Up to this point the center-line velocity is practically unaffected by mixing and substantially equal to the nozzle velocity, i.e. $\bar{V}_c/\bar{V}_{c,z/w=1} = 1$. Beyond the end of the so-called potential core the center-line velocity also diminishes as the jet shares its momentum with more and more entrained air. The present measurement of velocities has a similar trend as those of Gardon and Akfirat [16]. As for the distribution of turbulence intensity, the present turbulence along the center line of the jet generated by mixing is much more intense than that usually encountered in pipe flow, reaching levels of the order of 30%. The intensity of turbulence increases continuously with the distance measured from the nozzle exit. It should be noted as a matter of particular

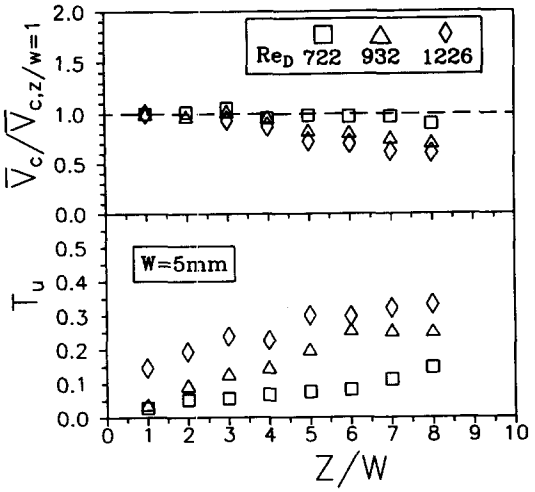

Fig. 7. Variation of velocity and turbulence intensity along the center line of the slot jet.

importance to the present considerations that the turbulence along the center line of the jet rises appreciably even before the axial velocity has begun to decline significantly.

According to the above-mentioned results, the slightly convex shape of heat transfer distribution can be observed due to the interaction of the turbulence intensity and the effect of H/W ratio. When the H/W ratio increases, the interaction region will increase. This leads to the enhancement of the heat transfer especially for the cases of a higher jet Reynolds number, say $Re_D = 1333$. On the other hand, the flow will be retarded which will result in the decay of turbulence intensity as the H/W ratio increases. Thus, the maximum value of the stagnation heat transfer in such a configuration is found at about $H/W \cong 3$ which is resulted from the competition of the turbulence intensity and the spatial effect. As for the cases of a lower jet Reynolds number, the enhancement of turbulence intensity is not so significant as that in a higher jet Reynolds number.

In addition, several existing results investigated by Gardon and Akfirat [16], Sparrow and Wong [15] and Al-Sanea [17] are plotted in Fig. 8 for comparisons with the present data of stagnation heat transfer characteristics. The comparison shows that the data of Al-Sanea are quite consistent with the present results, while those presented by Gardon and Akfirat and Sparrow and Wong are significantly deviated from the present results. The main reason is that, from the numerical study of Al-Sanea, the stagnation heat transfer characteristics are very sensitive to the jet velocity profile at slot-nozzle exit. The data of Al-Sanea evaluated with a uniform velocity distribution at nozzle exit are very close to the present results with a nozzle developing length of $L = 1.0$ W. On the contrary, the nozzle length of 76.1 W used by Sparrow and Wong is significantly larger than that in the present study. Thus, the heat transfer characteristics of stagnation line on the target surface may be enhanced with a parabolic profile at nozzle exit in Sparrow and Wong's study.

Furthermore, the comparisons of the present experimental data with the numerical results predicted by Chou and Hung [6] are illustrated in Fig. 9(a). The correlation of stagnation Nusselt number presented in Chou and Hung's study can be expressed as follows:

$$Nu_s = 5.574 Re_D^{0.5} (H/W)^{-0.17}. \quad (9)$$

The results evaluated with equation (9) are overpredicted since the effect of H/W is taken into consideration. Besides, the deviation between the experimental and numerical data becomes significant when $H/W = 1$. As mentioned above, the turbulence intensity as well as the three-dimensional effect may play an important role in determining heat transfer performance. Since the effect of H/W is insignificant in the present experiments, the relationship of stagnation Nusselt number and the jet Reynolds number can be correlated as:

$$Nu_s = 4.315 Re_D^{0.5}. \quad (10)$$

The average relative deviation of equation (10) from the experimental data is 4.56% with a maximum deviation 14.60% as shown in Fig. 9(b). The ranges of parametric validity for using equation (10) are $190 \leqslant Re_D \leqslant 1537$ and $1 \leqslant H/W \leqslant 8$.

Local heat transfer characteristics

Local Nusselt number variations along the heated target surface for the cases with various parameters and conditions are explored in the study. From the present results, the distribution of Nusselt number near the central symmetric region is zero-sloped and bell-like as stated by Hrycak [18]. In addition, as shown in Fig. 10, the local Nusselt number Nu_x increases with increasing jet Reynolds number. Furthermore, the present results also manifest that no significant change in the Nu_x distribution can be observed for the cases under different H/W and q_c'' values. As compared with the results reported in the existing literature, the present local Nusselt number distribution, which is more flat, is actually reasonable, especially for the cases of a low jet Reynolds number. This trend may be explained by the following reasons: (1) a strong effect of lateral heat conduction in X-direction can be found due to the high thermal conductivity of the AISI 304 stainless steel used as the impinged surface material. The reason to select an AISI 304 stainless steel as test material has been mentioned in the subsection of heated target block. That is, the thermal conductivity of AISI 304 ($k = 14.6$ W m K^{-1}) is almost the same order as that of alumina (Al_2O_3, $k = 18$–20 W m^{-1} K^{-1}) [8, 9]; (2) a more uniform temperature distribution can be obtained by the impingement of using a slot jet instead of a round jet [2]; (3) the length of the heated target surface in X direction in the present study is 6.7 mm, which is much

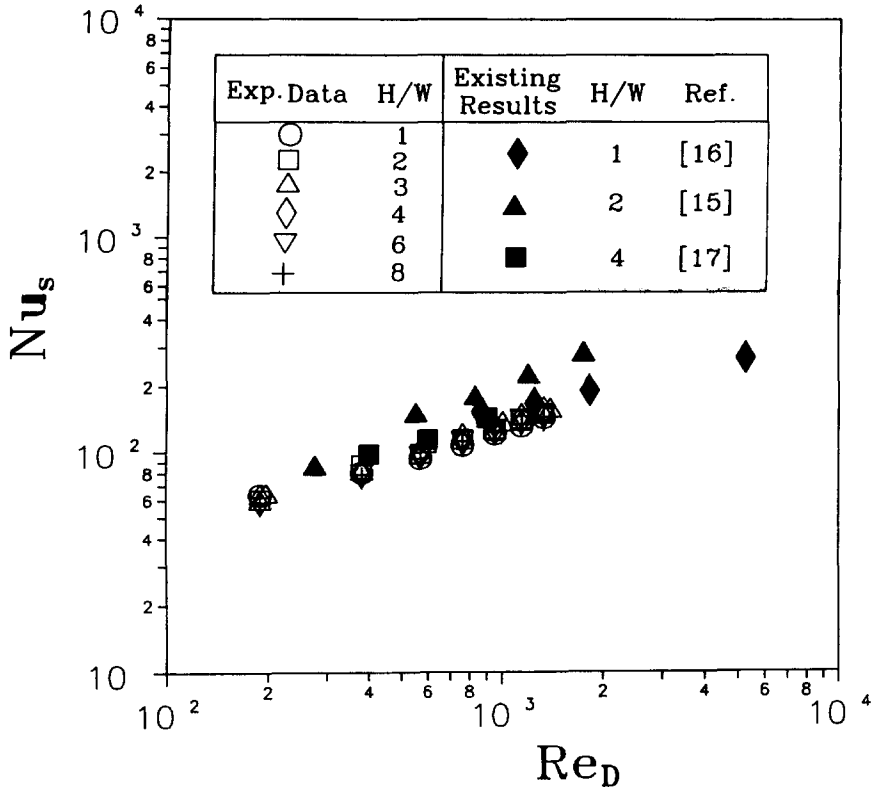

Fig. 8. Comparison of present experimental Nu_s data with existing results.

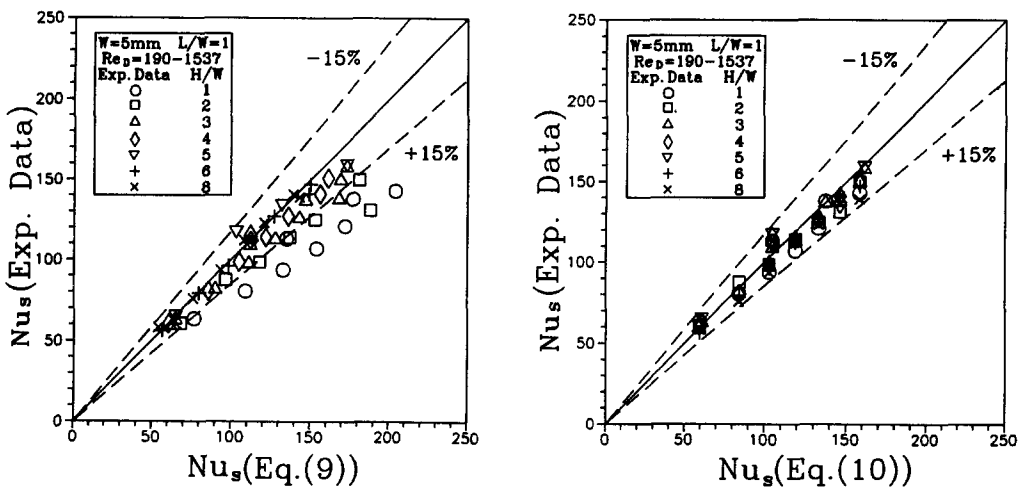

(a) Comparison of Exp. Data with Eq.(9)

(b) Comparison of Exp. Data with Eq.(10)

Fig. 9. Comparisons of present experimental Nu_s data with equations (9) and (10).

smaller than those studied in the existing literature. Therefore, the present results will be very valuable for the cooling design of MCM modules if a cooling method with slot jet impingement is employed.

Average heat transfer characteristics

As discussed in the stagnation heat transfer characteristics, the effects of H/W and q_c'' on average Nusselt numbers are insignificant in the present experiments, while the $\overline{Nu}$ data increase with increasing the jet Reynolds numbers. Consequently, a new correlation can be obtained in terms of jet Reynolds number based on the hydrodynamic diameter of the slot nozzle. It can be expressed as

$$\overline{Nu} = 3.755 Re_D^{0.5}. \quad (11)$$

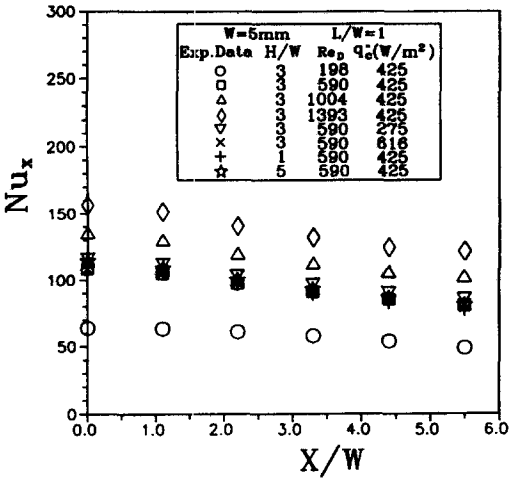

Fig. 10. Parametric effects on distribution of local Nusselt number.

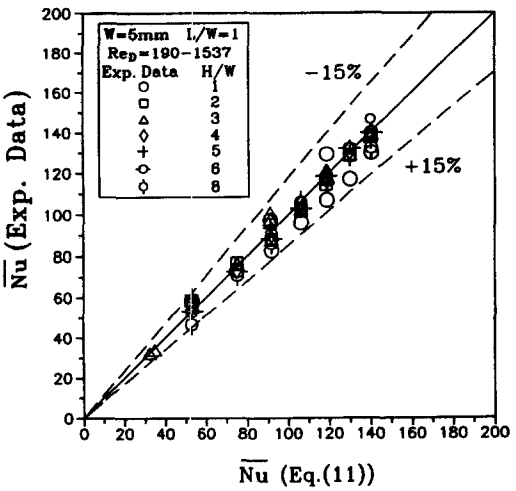

Fig. 11. Comparisons of present experimental data for average Nusselt number with equation (11).

The experimental results along with equation (11) are plotted in Fig. 11. The comparisons between the experimental data and the prediction are quite consistent with each other. The average deviation of equation (11) from the experimental results is 7.88% with a maximum relative deviation of 14.67%. If the relation of Prandtl number is taken into consideration, then equation (11) can be written as

$$\overline{Nu}/Pr^{1/3} = 4.229Re_D^{0.5} \tag{12}$$

where the validity of equation (12) is $Re_D = 190$–1537 and $H/W = 1$–8.

To compare with the existing study, the experimental results for the confined liquid jet (FC-72) carried out by Wadsworth and Mudawar [2] are also investigated. In their experiments, they correlated the experimental data using the superposition technique which subdivided the heat transfer surface into impingement and wall jet regions. The correlation recommended is of the form:

$$\overline{Nu}/Pr^{1/3} = 3.06Re_D^{0.5} + 0.099Re_D^{0.664}\,[(L_H - W)/W]^{0.664} \tag{13}$$

where equation (13) is based on data obtained over the ranges $1000 \leqslant Re_D \leqslant 30\,000$, $25 \leqslant L_H/W \leqslant 100$ and $1 \leqslant H/W \leqslant 20$.

Figure 12(a) shows the average Nusselt number based on the heater length versus the jet Reynolds number based on the slot hydrodynamic diameter. For a specified length of heater, the average Nusselt number based on the heater length can be easily evaluated. As shown in Fig. 12(a), the results exhibits that there are significant deviations among the correlations of Wadsworth and Mudawar [2], Chou and Hung [6] and the results of Schafer *et al.* [7] for the case of a short heater length such as $L_H/W = 4$. However, a good agreement between the results of Schafer *et al.* and the correlation of Chou and Hung for uniform wall temperature (UWT) cases is found. This is due to the validity of the correlation presented by Wadsworth and Mudawar, which was applied to the ranges of $H/W = 1$–20, $Re_D = 1000$–$30\,000$ and $L_H/W = 25$–100. Furthermore, the predicted values of UWT and UHF reported by Chou and Hung assure the two limiting conditions and are useful for practical design. As expected, the average Nusselt number of UHF case is usually higher than that of UWT case as demonstrated in Fig. 12(a).

In addition, the present experimental data are usually higher than the numerical results predicted by Chou and Hung [6]. It is not surprising because the discrepancies between calculated and measured results may be attributed to variable fluid properties, three-dimensional effects, the possible influence of buoyancy and/or turbulence in the experimental system [7]. In the study of Schafer *et al.* [7], the differences between the predicted and the measured results range from 16 to 44%. Furthermore, in Chou and Hung's numerical analysis [6], the conditions of transported properties are assured to be invariant in the flow direction at the outflow boundary. However, this assumption is not feasible in real experimental setup. When the jet fluid radially flows out from the finite-length confined channel, it suddenly expands. This leads to the acceleration of the fluid velocity. Accordingly, the measured data are generally higher than the predicted results in the downstream region of heated target surface. Besides, the local Nusselt number exponentially decays along the radial direction. The numerical average Nusselt number, which can be directly calculated by integrating the local performance along the streamwise heater length, is absolutely smaller than that evaluated with area-weighted values of discrete measured points in the experiment.

To avoid the above-mentioned discrepancy between experimental and numerical results, a concept of 'effective cooling length' proposed by Mohanty and Twafek [19] is introduced in the present study. In jet impingement problems, the distance measured from the stagnation line to a specified location where the

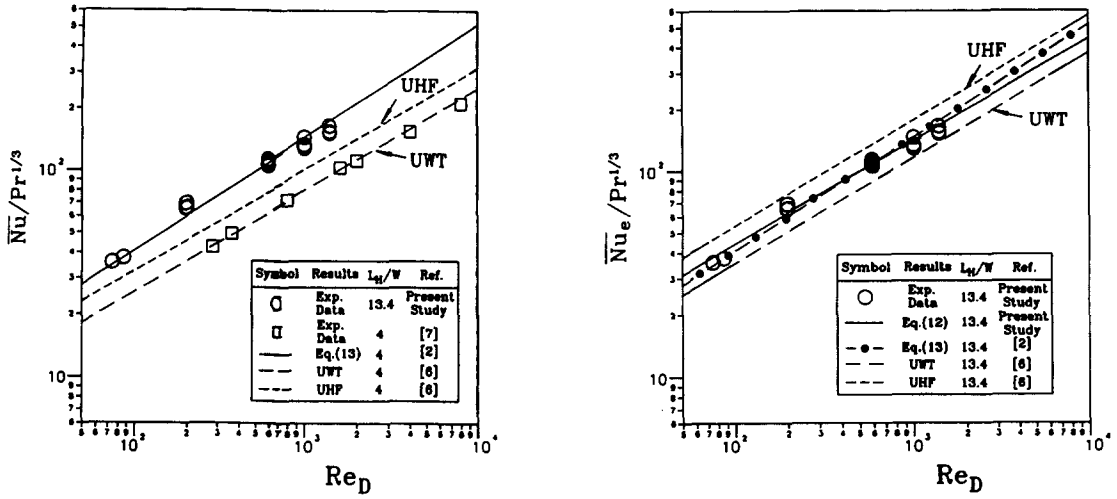

(a) Average Nusselt Number (b) Modified Average Nusselt Number

Fig. 12. Comparisons of average Nusselt number among present experimental data and existing correlations for $L_H/W = 4$ and $L_H/W = 13.4$.

heat transfer coefficient ratio, i.e. h_x/h_s, equals e^{-1} is defined as the effective cooling length, L_e. In other words, it can be expressed as

$$H_e = \frac{h_x}{h_s} = e^{-1} \quad \text{at} \quad X = L_e \tag{14}$$

where H_e is the effective cooling function.

Thus, the average heat transfer coefficient based on the effective cooling length can be easily evaluated with the following equation

$$\bar{h}_e = \frac{1}{L_e}\int_{L_e/2}^{L_e/2} h_x \, dX \tag{15}$$

where h_x is local heat transfer coefficient, which is obtained from the numerical results reported by Chou and Hung [6]. Accordingly, the modified average Nusselt number based on the length of heated target surface can be defined as

$$\overline{Nu}_e = \frac{\bar{h}_e L_H}{k}. \tag{16}$$

As for the cases with a long heater length of $L_H/W = 13.4$, the comparison of the present experimental data with equations (11) and (12) is made and shown in Fig. 12(b) with a satisfactory agreement. Besides, the numerical modified Nusselt numbers evaluated with equation (16) for UWT and UHF cases are also plotted in Fig. 12(b) for comparisons. It shows that the numerical modified Nusselt numbers predicted by equation (15) are well consistent with the present experimental data.

CONCLUSIONS

An experimental investigation of heat transfer behaviors of a confined slot jet impingement has been systematically performed in the present study. The main conclusions emerging from this study may be drawn as follows:

(1) The jet mean velocity profile at nozzle exit is developing in the present experiments. The entrainment effect of the jet itself and ambient fresh air is not significant when $Re_D < 1226$; while the jet is significantly affected by the ambient air when $Re_D \leqslant 1226$.

(2) All the turbulence intensities for the cases of $Re_D < 1226$ are less than 5% on the jet centerline at nozzle exit; accordingly, the jet at $Re_D < 1226$ can be regarded as in an initially laminar flow. As $Re_D \geqslant 1226$, it may be considered as in an initially transitional/turbulent regime because of an unsteady behavior with a significant high turbulence intensity for $Re_D \geqslant 1226$.

(3) The heat transfer characteristics, including stagnation, local and average Nusselt numbers, is significantly affected by jet Reynolds numbers; while it is insignificantly influenced by the ratio of jet separation distance to nozzle width.

(4) Two new empirical correlations of stagnation and average Nusselt numbers are proposed. The ranges of parametric validity for using this correlation are $190 \leqslant Re_D \leqslant 1537$ and $1 \leqslant H/W \leqslant 8$. The average relative deviations of these two correlations for stagnation and average Nusselt numbers from the corresponding experimental data are 4.56 and 7.88%, respectively.

(5) A concept of effective cooling length is intro-

duced for evaluating the numerical average heat transfer performance, the modified numerical predictions on the average Nusselt number presented by Chou and Hung [6] are consistent with the present experimental data.

Acknowledgement—The authors wish to thank the National Science Council, Taiwan, under the grant no. NSC82-0404-E-007-135, for their support.

REFERENCES

1. J. W. Hoyt, and J. J. Taylor, Effect of nozzle boundary layer on water jets discharging in air, *Jet and Cavities—Int. Symp.*, pp. 93–100. ASME, New York (1985).
2. D. C. Wadsworth and I. Mudawar, Cooling of a multichip electronic module by means of confined two-dimensional jets of liquid, *ASME J. Heat Transfer* **112,** 891–898 (1990).
3. M. L. Minges, *Electronic Materials Handbook Volume 1 : Packaging*, pp. 46–49. ASM International, Materials Park, OH (1989).
4. S. Polat, B. Huang, A. S. Mujumdar and W. J. M. Douglas, Numerical flow and heat transfer under impinging jets : a review, In : *Annual Review of Numerical Fluid Mechanics and Heat Transfer* (Edited by C. L. Tien and T. C. Chawla), Vol. 2, pp. 157–197. Hemisphere, New York (1989).
5. Y. J. Chou and Y. H. Hung, Hydrodynamic characteristics of a confined slot jet impingement, *J. Chin. Soc. Mech. Engng* **15,** 71–78 (1994).
6. Y. J. Chou and Y. H. Hung, Impingement cooling of an isothermally heated surface with a confined slot jet, *ASME J. Heat Transfer* **166,** 479–482 (1994).
7. D. M. Schafer, F. P. Incropera and S. Ramadhyani, Numerical simulation of laminar convection heat transfer from an in-line array of discrete sources to a confined rectangular jet, *Numer. Heat Transfer A* **22,** 121–141 (1992).
8. F. P. Incropera and D. P. Dewitt, *Fundamentals of Heat and Mass Transfer*, 2nd Edn, pp. 755–757. Purdue University, Indiana (1985).
9. R. R. Tummala and E. J. Rymaszewski (ed.), *Microelectronic Packaging Handbook*, p. 36. Van Nostrand Reinhold, New York (1989).
10. C. S. Tsai, Transient heat transfer characteristics of a round jet impingement, Master's Thesis, Department of Power Mechanical Engineering, National Tsing Hua University, Taiwan (1994).
11. S. J. Kline and F. A. McClintock, Describing uncertainties in single-sample experiments, *Mech. Engng* 3–8 (1953).
12. R. J. Moffat, Describing the uncertainties in experimental results, *Expl Therm. Fluid Sci.* **1,** 3–17 (1988).
13. J. A. Schetz, *Boundary Layer Analysis*, Prentice Hall, New Jersey (1993).
14. K. J. McNaughton and C. G. Sinclair, Submerged jets in short cylindrical vessels, *J. Fluid Mech*, **25,** 367–375 (1966).
15. E. M. Sparrow and T. C. Wong, Impingement transfer coefficients due to initially laminar slot jets, *Int. J. Heat Mass Transfer* **18,** 597–605 (1975).
16. R. Gardon and J. C. Akfirat, Heat Transfer characteristics of impinging two-dimensional air jets, *ASME J. Heat Transfer* **88,** 101–108 (1966).
17. S. Al-Sanea, A numerical study of the flow and heat transfer characteristics of an impinging laminar slot-jet including crossflow effects, *Int. J. Heat Mass Transfer* **35,** 2501–2513 (1992).
18. P. Hrycak, Heat Transfer from impinging jets to a flat plate, *Int. J. Heat Mass Transfer* **26,** 1857–1865 (1983).
19. A. K. Mohanty and A. A. Twafek, Heat transfer due to a round jet impinging normal to a flat surface, *Int. J. Heat Mass Transfer* **36,** 1639–1647 (1993).